Composite Structures 319 (2023) 117147

Contents lists available at ScienceDirect

Composite Structures

journal homepage: www.elsevier.com/locate/compstruct

A nonlocal method to compute effective properties of viscoelastic composite materials based on peridynamic computational homogenization theory

Yakubu Kasimu Galadima [a,b], Selda Oterkus [a,*], Erkan Oterkus [a], Islam Amin [a,c], Abdel-Hameed El-Aassar [d], Hosam Shawky [d]

[a] PeriDynamics Research Centre, Department of Naval Architecture, Ocean and Marine Engineering, University of Strathclyde, Glasgow, United Kingdom
[b] Department of Civil Engineering, Ahmadu Bello University, Zaria, Nigeria
[c] Department of Naval Architecture and Marine Engineering, Port Said University, Port Said, Egypt
[d] Egypt Desalination Research Centre of Excellence (EDRC) and Hydrogeochemistry Department, Desert Research Centre, Cairo, Egypt

ARTICLE INFO

Keywords:
Peridynamics
Viscoelasticity
Composite materials
Non-ordinary State-based
Nonlocal

ABSTRACT

This article presents a computational homogenization framework for viscoelastic composites within the framework of non-ordinary state-based peridynamic theory. The motivation to develop this framework stems from the desire to develop a homogenization scheme that can model processes and phenomena that are driven by nonlocal behaviour such as size effect and fracture for which frameworks based on the classical continuum theory lack the capability of modelling. The proposed framework was used to calculate the effective properties in both time and frequency domains of two viscoelastic matrix-inclusion composite systems, one with an elastic inclusion and viscoelastic matrix, and the other with viscoelastic inclusion and matrix. The results of calculations were found to compare well with results from the literature. A parametric study was also conducted to investigate the influence of nonlocal interaction on the effective properties by varying the horizon size. Results showed that increasing the degree of nonlocality reduces the stiffness of the composite system as well as increase its rate of creep. The capability to account for nonlocal interaction highlights the potential of this proposed scheme to provide a more comprehensive understanding of the behaviour of viscoelastic composite materials over a wide range of material behaviour.

1. Introduction

The design and optimization of viscoelastic composite materials is an important and growing area of research in materials science and engineering. The increasing acceptability of viscoelastic composite materials in industries such as civil, aerospace, automotive, and biomedical engineering is partly due to the advantage it offers designers and engineers to tailor its microstructure to achieve optimal overall or 'effective' performance. This is achieved not only through choosing the optimal parameters of the constituent materials but also choosing the optimal layout and arrangement of the constituent materials.

Computational homogenization schemes are a popular method for characterizing the properties of viscoelastic composite materials. These schemes are numerical frameworks that are used to predict the effective properties of a composite material by simulating the behaviour of the individual constituent materials and their interactions at the subscale. Traditionally, most computational homogenization schemes for analysis of composite systems [1-3] in general and viscoelastic composite systems [4,5] in particular, have been developed based on classical continuum mechanics, which is built upon the assumption of local action as well as smooth and continuous deformation. However, there are many mechanisms that give rise to processes in composite materials which invalidate these fundamental assumptions of the classical theory.

Discontinuous material behaviour, such as fracture, presents a significant challenge for modelling within the framework of classical continuum mechanics. This is because the theory relies on spatial derivatives to describe physical system which necessarily impose the conditions of smooth and continuous deformation on the material. This mathematical framework is not suitable for modelling fracture processes such as brittle fracture and fragmentation [6].

* Corresponding author.
E-mail address: selda.oterkus@strath.ac.uk (S. Oterkus).

https://doi.org/10.1016/j.compstruct.2023.117147
Received 25 January 2023; Received in revised form 18 April 2023; Accepted 10 May 2023
Available online 16 May 2023

Strain localization in materials that exhibit strain softening due to damage is another problem that is difficult to model using the classical continuum theory. Using the classical framework to model such phenomenon presents two problems. The first is the non-uniqueness of the result due to the loss of ellipticity of the governing differential equations of the classical theory and the second is a numerical problem that typically manifest as the spurious localization of strain into a narrow band that is dependent on grid size of the numerical scheme, e.g. element size in finite element model [7]. As a result, it is deemed inappropriate to utilise models based on the classical continuum framework to characterise materials that exhibit strain-softening behaviour [7,8].

Crazing is a key mechanism of deformation in polymers, which is characterized by the nucleation and propagation of small cracks at the surface of the material. The size of the specimen plays a crucial role in the behaviour of crazed polymers. This is because as the specimen size decreases, the probability of craze nucleation at the surface increases, leading to more deformation. Thus, the larger the ratio of surface to volume in the specimen, the more likely it is for crazes to nucleate and propagate, leading to a decrease in the mechanical strength of the material. This is a manifestation of a more general phenomenon known as size effect. Size effect is known to be notoriously difficult to model in the framework of the classical theory. This is because the resolution of this effect require a length scale parameter to be present in the constitutive model [9]. Unfortunately, such a parameter does not exist in the constitutive model of the classical theory.

Considering these challenges many attempts have been made to develop continuum theories with extended capabilities to overcome these limitations. The result of one of such attempts is the peridynamic theory which provided a one stop solution to all the limitation of the classical theory highlighted above. The peridynamic theory overcomes the problem of modelling discontinuous behaviour by replacing the spatial derivatives with integral operators thereby eliminating the requirement for the smoothness and continuity conditions. As a result of this capability, peridynamics have been extensively applied to characterise materials undergoing fracture and other discontinuous processes [10,11].

In peridynamics, the force acting at a point is defined as an integral over a finite neighbourhood called the influence domain. The force density integral operator introduces a notion of horizon into the peridynamic model. If the influence domain is taken to be a sphere, then the radius of the sphere is designated as the horizon. All material points that lie within the domain of influence of a point are said to belong to its family. The nonlocality of force interaction which allow a point to interact with other points located within its horizon endows peridynamic with nonlocal characteristics, and the horizon is the parameter that controls the degree of nonlocality in the peridynamic theory. The horizon not only endows peridynamics with nonlocal characteristics but also introduces the notion of internal length scale into the peridynamic framework [12,13], thus making peridynamics a viable continuum theory for modelling phenomena such as size effects [14]. Endowed with the forgoing capabilities, peridynamics continues to attract growing interest from researchers across different disciplines and have been applied to study a wide spectrum of engineering problems, see [15-34].

A critical frontier of computational modelling of material in the PD framework that is steadily receiving attention form researchers is the development of nonlocal homogenization schemes for the characterisation of heterogeneous materials such as composites and materials with important microstructure. In this regard, several homogenization theories for PD have been proposed. One such method is the Peridynamic unit cell homogenization method proposed in [35] and involves using a strain concentration tensor to establish the coupling between the micro and macro scales. The strain concentration tensor is a function that considers the geometry and constitutive properties of the materials that make up a unit cell, and it is used to describe the fluctuations in micro-strain in relation to the average strain at the macro scale. To determine the components of this tensor, an equilibrium problem is solved by imposing periodic boundary conditions on the unit cell. The method assumes that the heterogeneous medium has a periodic microstructure.

Several peridynamic homogenization methods that are based on the concept of strain energy equivalence have been proposed and used in various publications. These methods posit that two materials with different microstructures can be considered constitutively equivalent if they have the same strain energy when subjected to affine deformation. In this regard, a homogenization theory in the framework of Bond-based PD was proposed in [36] for computation of the effective properties of composites. An ordinary state-based peridynamic homogenization was proposed in [37] to characterise the behaviour of composite materials. In [38], the capability of PD to admit constitutive models from CCM was explored to develop a peridynamic computational homogenization theory (PDCHT) in the non-ordinary state-based framework to study the behaviour of composites. This method was further utilised to study the behaviour of materials with evolving microstructure in [39].

The homogenization schemes discussed above were only applied to characterise materials which exhibit elastic behaviour. However, many composite materials, especially those containing polymers, exhibit time- and rate-dependent behaviour that cannot be accurately described by elasticity theory alone. These materials experience creeping deformations, relaxed stresses, and damped mechanical vibrations. Because they display both viscous and elastic characteristics, these materials are referred to as viscoelastic. On the one hand, viscoelastic materials are increasingly finding application across a wide spectrum of industries including automobile, aerospace, civil and biomedical engineering. On the other hand, it has been established that there exist many problems for which computational frameworks based on the CCM is unable to produce any meaningful predictions, such as size-scale effects which is observed particularly in the field of micro and nanomaterials and microstructural effects arising from the arrangement of grains or the distribution of defects in polymers.

Motivated by the capability of PD to capture the size-scale effects and nonlocal spatial interactions in composites [40], quasi-brittle materials [14] and bilayered systems [41], this study presents a numerical modelling method that utilizes the PDCHT proposed in [38] to assess the influence of microscopic variations on the macroscopic response of viscoelastic composites. This method involves solving boundary value problems in a microscopic domain to calculate a homogenized stiffness based on the microstructure of the composite. The PD model represents the material as a network of bonds that interact via a nonlocal interaction kernel, allowing for the capture of nonlocal effects and the prediction of the effective properties of the composite.

The remainder of this article is organized as follows. In the next section, we provide a brief overview of the peridynamic model and its application to the analysis of viscoelastic composites. We then describe the proposed homogenization framework in detail, including the mathematical formulation and the numerical algorithms used to solve the resulting equations. Finally, we present some numerical examples to demonstrate the effectiveness of the proposed method and to compare its results with those obtained using other approaches.

2. Non-ordinary state-based peridynamics and viscoelastic constitutive model

The mathematical basis of peridynamic theory is centred around the concept of a bond, which represents the nonlocal interaction between two points in a material. Let $\mathscr{B}$ in Fig. 1 be a deformable body such that $\mathscr{B}_0$ and $\mathscr{B}_t$ represent the reference and deformed configurations of $\mathscr{B}$, respectively. Let $\boldsymbol{P}$ be a point in $\mathscr{B}$ such that $\boldsymbol{P}$ is identified by its coordinate vector $\mathbf{x}$ in $\mathscr{B}_0$ and let the coordinate vector of $\boldsymbol{P}$ in $\mathscr{B}_t$ be $\mathbf{y}$. The PD theory posit that the interaction domain of $\mathbf{x}$ extend beyond the set of points in contact with $\mathbf{x}$ to include points located at a finite distance from $\mathbf{x}$. Let $\boldsymbol{Q}$ be another point in $\mathscr{B}$ such that $\boldsymbol{Q}$ is identified by its coordinate

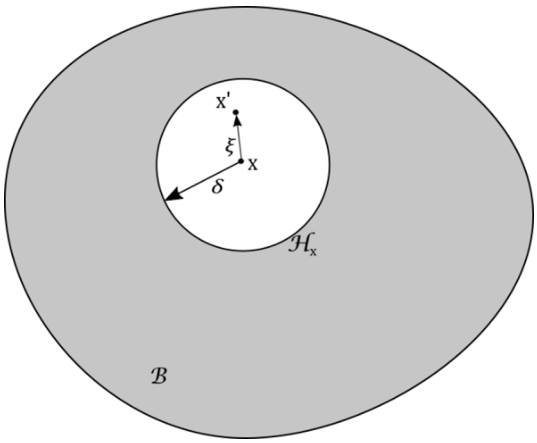

Fig. 1. A peridynamic body showing nonlocal interaction between points.

vector $\mathbf{x}'$ in $\mathscr{B}_0$ and let the coordinate vector of $\boldsymbol{Q}$ in $\mathscr{B}_t$ be $\boldsymbol{y}'$. The set of all $\mathbf{x}' \in \mathscr{B}$ that interacts with $\mathbf{x}$ is called the family of $\mathbf{x}$. If the region occupied by this set is assumed to be a ball of radius $\delta > 0$ that is centered at $\mathbf{x}$ then the family of $\mathbf{x}$ is defined as

$$\mathscr{B}_\delta(\mathbf{x}) = \{\mathbf{x}' \in \mathscr{R} : |\mathbf{x}' - \mathbf{x}| < \delta\} \tag{1}$$

The interaction between $\mathbf{x}$ and $\mathbf{x}'$ is called a *bond*, and the distance $\boldsymbol{\xi} = \mathbf{x}' - \mathbf{x}$ between them in the undeformed configuration is referred to as the *bond length* (also called bond for short so that precise meaning is clear from the context). The set of bonds for point $\mathbf{x}$, denoted as $\mathscr{H}_\mathbf{x}$, is given as

$$\mathscr{H}_\mathbf{x} = \{\boldsymbol{\xi} \in (\mathbb{R}\backslash 0) | (\boldsymbol{\xi} + \mathbf{x}) \in (\mathscr{B}_\delta(\mathbf{x}) \cap \mathfrak{B})\} \tag{2}$$

Let $\mathbf{F} : \mathscr{B}_0 \rightarrow \mathscr{B}_t$ be the nonlocal deformation gradient that maps $\mathbf{x}$ to $\mathbf{y}$ and $\mathbf{x}'$ to $\mathbf{y}'$, respectively, so that $\boldsymbol{u}(\mathbf{x}) = \mathbf{y} - \mathbf{x}$ and $\boldsymbol{u}(\mathbf{x}') = \mathbf{y}' - \mathbf{x}'$ represent the displacements undergone by $\mathbf{x}$ and $\mathbf{x}'$, respectively, therefore, the relative displacement between $\mathbf{x}$ and $\mathbf{x}'$ is expressed as $\boldsymbol{\eta} = \boldsymbol{u}(\mathbf{x}') - \boldsymbol{u}(\mathbf{x})$.

The equation of motion of material point $\mathbf{x}$ as it interacts with all points $\mathbf{x}'$ belonging to its family is given by the linear momentum Eq. [6]

$$\rho\ddot{\boldsymbol{u}}(\mathbf{x}) = \int_{\mathscr{B}_\delta(\boldsymbol{x})} \mathbf{f}(\mathbf{x}, \mathbf{x}') d\mathbf{x}' + \boldsymbol{b}(\mathbf{x}, t) \tag{3}$$

where $\ddot{\boldsymbol{u}}$ is the second order time derivative of the displacement at $\mathbf{x}$, $\boldsymbol{b}$ is the prescribed body force density at $\mathbf{x}$, and $\mathbf{f}$ is a vector valued pairwise bond force density that point $\mathbf{x}'$ exerts on $\mathbf{x}$. The specific form of $\mathbf{f}$ depends on the complexity of the material model adopted. The bond-based model is the most basic type of peridynamic model in which $\mathbf{f}(\mathbf{x}, \mathbf{x}')$ is only dependent on the deformation of the bond $\mathbf{x}' - \mathbf{x}$. Although the easiest PD model, the BBPD suffers from the limitation of admitting Poisson's ratio of $1/3$ and $1/4$ for 2- and 3-D problems, respectively for isotropic materials. State-based peridynamic (SBPD) models offer a more generalised modelling framework in which $\mathbf{f}(\mathbf{x}, \mathbf{x}')$ does not only depend on the bond $\mathbf{x}' - \mathbf{x}$, but rather on all bonds in $\mathscr{H}_\mathbf{x}$. This allows for a more generalized representation of material behaviour beyond the capability of the BBPD.

To achieve this extended capability, the SBPD introduces mathematical objects called *states*, which are functions defined on bonds. Let $\mathscr{L}_m$ be the set of all order m tensors, then a state $\underline{\boldsymbol{A}}$ of order m associated with the bond $\mathscr{H}$ is the function $\underline{\boldsymbol{A}}\langle\bullet\rangle : \mathscr{H} \rightarrow \mathscr{L}_m$, where the angle bracket signify the bond acted upon by the state. Thus, the bond force density $\mathbf{f}(\mathbf{x}, \mathbf{x}')$ in the SBPD is given by

$$\mathbf{f}(\mathbf{x}, \mathbf{x}') = \underline{\mathbf{T}}[\mathbf{x}]\langle\mathbf{x}' - \mathbf{x}\rangle - \underline{\mathbf{T}}[\mathbf{x}']\langle\mathbf{x} - \mathbf{x}'\rangle = \mathbf{t}(\mathbf{x}', \mathbf{x}, t) - \mathbf{t}(\mathbf{x}, \mathbf{x}', t) \tag{4}$$

where $\underline{\mathbf{T}}[\mathbf{x}]$ is the force vector state acting at $\mathbf{x}$ whose value acting on the bond $\boldsymbol{\xi} = \mathbf{x}' - \mathbf{x}$ is the force density vector $\mathbf{t}(\mathbf{x}', \mathbf{x}, t)$ acting on $\mathbf{x}$ due to its interaction with $\mathbf{x}'$ and $\underline{\mathbf{T}}[\mathbf{x}']$ is the force vector state acting at $\mathbf{x}'$ whose value acting on the bond $\boldsymbol{\xi}' = \mathbf{x} - \mathbf{x}'$ is the force density vector $\mathbf{t}(\mathbf{x}, \mathbf{x}', t)$ acting on $\mathbf{x}'$ due to its interaction with $\mathbf{x}$. By substituting (4) into (3), the governing equation of motion in the SBPD framework is given by

$$\rho\ddot{\boldsymbol{u}}(\mathbf{x}) = \int_{\mathscr{B}_\delta(\boldsymbol{x})} \left[\underline{\mathbf{T}}[\mathbf{x}]\langle\mathbf{x}' - \mathbf{x}\rangle - \underline{\mathbf{T}}[\mathbf{x}']\langle\mathbf{x} - \mathbf{x}'\rangle\right] d\mathbf{x}' + \boldsymbol{b}(\mathbf{x}, t) \tag{5}$$

On the kinematic front, a reference position vector state $\underline{\mathbf{X}}$ is defined as a vector state that maps bonds in $\mathscr{B}_0$ unto themselves, that is for the bond $\boldsymbol{\xi}$

$$\underline{\mathbf{X}}[\mathbf{x}]\langle\mathbf{x}' - \mathbf{x}\rangle = \mathbf{x}' - \mathbf{x} = \boldsymbol{\xi} \tag{6}$$

Another important kinematic state to be defined here is the deformation vector state $\underline{\mathbf{Y}}$ whose value acting on the bond $\boldsymbol{\xi}$ is the image of $\boldsymbol{\xi}$ in $\mathscr{B}_t$, such that

$$\underline{\mathbf{Y}}[\mathbf{x}, t]\langle\mathbf{x}' - \mathbf{x}\rangle = \mathbf{y}'(\mathbf{x}', t) - \mathbf{y}(\mathbf{x}, t)$$

$$= \boldsymbol{u}(\mathbf{x}', t) - \boldsymbol{u}(\mathbf{x}, t) + \boldsymbol{\xi} \tag{7}$$

The relationship between the deformation state $\underline{\mathbf{Y}}$ and the nonlocal deformation gradient $\mathbf{F}$ for small perturbation hypothesis is obtained by taking a Taylor series expansion of (7) to obtain:

$$\underline{\mathbf{Y}}[\mathbf{x}, t]\langle\mathbf{x}' - \mathbf{x}\rangle = (\mathscr{G}_{\omega_\mathbf{x}}\boldsymbol{u}(\mathbf{x}) + \mathbf{I}) \bullet \boldsymbol{\xi}$$

$$= \mathscr{G}_{\omega_\mathbf{x}}\mathbf{y}(\mathbf{x}) \bullet \boldsymbol{\xi}$$

$$= \mathbf{F} \bullet \boldsymbol{\xi} \tag{8}$$

where $\mathscr{G}$ denotes the nonlocal gradient operator [38], and the nonlocal deformation gradient is given by [42]

$$\mathbf{F}(\mathbf{x}) = \left[\int_{\mathbb{R}^n} \omega(|\boldsymbol{\xi}|)(\mathbf{y}(\mathbf{x}', t) - \mathbf{y}(\mathbf{x}, t)) \otimes \boldsymbol{\xi} d\mathbf{x}'\right] \mathbf{K}^{-1} \tag{9}$$

In (9), $\mathbf{K}$ is a second order tensor defined as

$$\mathbf{K} = \int_{\mathscr{H}_\mathbf{x}} \underline{\omega}\langle\boldsymbol{\xi}\rangle \underline{\mathbf{X}}\langle\boldsymbol{\xi}\rangle \otimes \underline{\mathbf{X}}\langle\boldsymbol{\xi}\rangle dV_\xi \tag{10}$$

The forgoing allows for the definition of a nonlocal strain tensor as

$$\mathbf{E} = \frac{1}{2}(\mathbf{F}^T\mathbf{F} - \mathbf{I}) \tag{11}$$

where $\mathbf{E}$ is the nonlocal analogue of the Green-Lagrange tensor which under small perturbation hypothesis reduces to

$$\mathbf{E} \approx \varepsilon = \frac{1}{2}(\mathbf{F} + \mathbf{F}^T) - \mathbf{I} \tag{12}$$

In (12), ε is the infinitesimal strain tensor and $\mathbf{I}$ is the second order isotropic tensor. Expressions (6)-(12) gives the nonlocal kinematic quantities needed to describe the motion of a point.

To complete the development of the volume constrained problem (VCP) (the analogue of the local boundary value problem (BVP) in the

nonlocal framework), a constitutive material model $\underline{\widehat{\mathbf{T}}}$ is required that will relate the force vector state $\underline{\mathbf{T}}$ with (the appropriate kinematic quantity) the deformation vector state $\underline{\mathbf{Y}}$, such that:

$$\underline{\mathbf{T}}[\mathbf{x},t] = \underline{\widehat{\mathbf{T}}}\left[\underline{\mathbf{Y}}[\mathbf{x},t]\right] \tag{13}$$

Two class of material model arises from (13). When $\underline{\widehat{\mathbf{T}}}$ is such that $\underline{\mathbf{T}}$ and $\underline{\mathbf{Y}}$ are colinear, then $\underline{\widehat{\mathbf{T}}}$ is said to be an ordinary state-based peridynamic (OSBPD) material model, otherwise $\underline{\widehat{\mathbf{T}}}$ is said to be non-ordinary state-based peridynamic (NOSBPD) material model [42]. In this contribution, the NOSBP will be used as the material model. One approach [43] to determine the functional form of the material model $\underline{\widehat{\mathbf{T}}}$ results to a correspondence NOSBPD material model which admits constitutive material models from the CCM. In this framework, following from [42], the force density vector is given by the following expression

$$\underline{\mathbf{T}}[\mathbf{x},t]\langle\boldsymbol{\xi}\rangle = \omega(|\boldsymbol{\xi}|)\mathbf{P}\mathbf{K}^{-1}\boldsymbol{\xi} \tag{14}$$

where ω is a scalar valued influence function and $\mathbf{P} = \widehat{\mathbf{P}}(\mathbf{F})$ is the first Piola-Kirchhoff stress tensor obtained through the response function $\widehat{\mathbf{P}}$ from CCM. If small perturbation hypothesis is made, then the Piola-Kirchhoff stress tensor $\mathbf{P}$ approximates to the Cauchy stress tensor $\boldsymbol{\sigma}$ such that $\boldsymbol{\sigma} \cong \mathbf{P} = \widehat{\mathbf{P}}(\mathbf{F})$, and (13) can be restated as:

$$\underline{\mathbf{T}}[\mathbf{x},t]\langle\boldsymbol{\xi}\rangle = \omega(|\boldsymbol{\xi}|)\boldsymbol{\sigma}\mathbf{K}^{-1}\boldsymbol{\xi} \tag{15}$$

3. Zero energy mode suppression

Despite the many advantages offered by the non-ordinary state-based peridynamic correspondence model, its solution often exhibits instability in the displacement field. This is mainly due to the inability of the nonlocal deformation gradient of the non-ordinary state-based constitutive correspondence framework to detect certain unphysical deformation modes [44]. These unphysical deformation modes, also called zero-energy modes (because no strain energy is required to produce them), need to be supressed. Several techniques [45-51] have been proposed to supress the resultant instability. For reason of ease of implementation, this study will adopt the approach proposed in [49]. This method prevents the zero-energy mode instability by adding an artificial force density vector $\underline{\mathbf{T}}_a[\mathbf{x},t]\langle\mathbf{x}' - \mathbf{x}\rangle$ to the interaction between $\mathbf{x}$ and $\mathbf{x}'$ such that (15) becomes:

$$\underline{\mathbf{T}}\langle\boldsymbol{\xi}\rangle = \underline{\omega}\langle|\boldsymbol{\xi}|\rangle\boldsymbol{\sigma}\mathbf{K}^{-1}\boldsymbol{\xi} + \underline{\mathbf{T}}_a[\mathbf{x},t]\langle\mathbf{x}' - \mathbf{x}\rangle \tag{16}$$

where:

$$\underline{\mathbf{T}}_a[\mathbf{x},t]\langle\mathbf{x}' - \mathbf{x}\rangle = \frac{1}{2}\underline{\omega}\langle|\boldsymbol{\xi}|\rangle\boldsymbol{C}\underline{z}\langle\boldsymbol{\xi}\rangle \tag{17}$$

In (17), $\boldsymbol{C}(\boldsymbol{\xi}) = c(\boldsymbol{\xi}\otimes\boldsymbol{\xi})/|\boldsymbol{\xi}|^3$ is a tensor-valued symmetric micro-modulus function where $c = 18k/\pi\delta^4$ is the bond force constant in the BBPD framework, and $\underline{z}\langle\boldsymbol{\xi}\rangle = \underline{\mathbf{Y}}\langle\boldsymbol{\xi}\rangle - \mathbf{F}\boldsymbol{\xi}$.

4. Linear viscoelastic constitutive model

The constituents of the composites studied in this communication will be assumed to be isotropic and linear in behaviour. From (14) and (15), it is clear that the NOSBPD can admit a wide range of constitutive models from CCM, and the response function adopted will depend on the type of material behaviour anticipated. Since the goal in this communication is to extend the PDCHT to encompass viscoelastic materials, this section will introduce the concept of viscoelastic constitutive model from the CCM and derive a form of the constitutive model that can be easily and efficiently implemented within the NOSBPD computational framework. There are two main approaches to developing viscoelastic models in CCM: the integral approach and the differential approach. Only the integral approach will be pursued in this contribution. The response function in the integral form for a linear non-ageing viscoelastic material takes the form:

$$\sigma_{ij}(t) = \int_0^t C_{ijkl}(t-\tau)\frac{d}{d\tau}\varepsilon_{kl}(\tau)d\tau \tag{18}$$

where $C_{ijkl}(t-\tau)$ is the fourth order stress relaxation stiffness tensor. The relaxation stiffness tensor is typically approximated by a series of decaying exponents also called Prony series such that:

$$C_{ijkl}(t) = C_{ijkl_\infty} + \sum\nolimits_{m=1}^{n} C_{ijkl_m}\exp\left(-\frac{t}{\tau_m}\right) \tag{19}$$

where the first term, C_{ijkl_∞} is the equilibrium or elastic modulus of the material while each subsequent term in the series represent a relaxation mode of the material. Introducing (19) into (18) yields

$$\begin{aligned}\sigma_{ij}(t) &= \int_0^t C_{ijkl_\infty}\frac{d}{d\tau}\varepsilon_{kl}(\tau)d\tau + \sum_{m=1}^{n}\int_0^t C_{ijkl_m}\exp\left(-\frac{t-\tau}{\tau_m}\right)\frac{d}{d\tau}\varepsilon_{kl}(\tau)d\tau \\ &= C_{ijkl_\infty}\varepsilon_{kl}(t) + \sum_{m=1}^{n}\int_{-\infty}^t C_{ijkl_m}\exp\left(-\frac{t-\tau}{\tau_m}\right)\frac{d}{d\tau}\varepsilon_{kl}(\tau)d\tau \\ &= \sigma_{ij_\infty}(t) + \sum_{m=1}^{n} h_{ij_m}(t)\end{aligned} \tag{20}$$

where $\sigma_{ij_\infty}(t) = C_{ij_\infty}\varepsilon_{kl}(t)$ represents the elastic component of the material response, and

$$h_{ij_m}(t) = \int_0^t C_{ijkl_m}\exp\left(-\frac{t-\tau}{\tau_m}\right)\frac{d\varepsilon_{kl}(\tau)}{d\tau}d\tau \tag{21}$$

commonly referred to as *state variable* is the viscous response of the material. Notice that to obtain the stress at a particular time, the constitutive relationship given by (20) leads to the requirement of computing the integral in (21). This is not suitable for implementation in a numerical scheme as this will require the entire history of the deformation to be stored. This is obviously not a computationally efficient strategy. To obtain a computationally more efficient form of (20), numerical incremental procedure is normally utilised. To achieve this, the loading time t is divided into discrete interval Δt such that $t_{n+1} = t_n + \Delta t$. Now, considering the time interval $[t_n, t_{n+1}]$, the deformation history can be split into two periods of $0 \le \tau \le t_n$ of known deformation and $t_n \le \tau \le t_{n+1}$ of unknown deformation. The integral in (21) can then be additively split into:

$$h_{ij}^{n+1}m = \int_0^{t_n} C_{ijkl_m}\exp\left(-\frac{t_{n+1}-\tau}{\tau_m}\right)\frac{d\varepsilon_{kl}(\tau)}{d\tau}d\tau + \int_{t_n}^{t_{n+1}} C_{ijkl_m}\exp\left(-\frac{t_{n+1}-\tau}{\tau_m}\right)\frac{d\varepsilon_{kl}(\tau)}{d\tau}d\tau$$

$$= \int_0^{t_n} C_{ijkl_m}\exp\left(-\frac{t_n+\Delta t-\tau}{\tau_m}\right)\frac{d\varepsilon_{kl}(\tau)}{d\tau}d\tau + \int_{t_n}^{t_{n+1}} C_{ijkl_m}\exp\left(-\frac{t_{n+1}-\tau}{\tau_m}\right)\frac{d\varepsilon_{kl}(\tau)}{d\tau}d\tau$$

$$= \int_0^{t_n} C_{ijkl_m}\exp\left(-\frac{\Delta t}{\tau_m}\right)\exp\left(-\frac{t_n-\tau}{\tau_m}\right)\frac{d\varepsilon_{kl}(\tau)}{d\tau}d\tau + \int_{t_n}^{t_{n+1}} C_{ijkl_m}\exp\left(-\frac{t_{n+1}-\tau}{\tau_m}\right)\frac{d\varepsilon_{kl}(\tau)}{d\tau}d\tau$$

$$= \exp\left(-\frac{\Delta t}{\tau_m}\right)\int_0^{t_n} C_{ijkl_m}\exp\left(-\frac{t_n-\tau}{\tau_m}\right)\frac{d\varepsilon_{kl}(\tau)}{d\tau}d\tau + \int_{t_n}^{t_{n+1}} C_{ijkl_m}\exp\left(-\frac{t_{n+1}-\tau}{\tau_m}\right)\frac{d\varepsilon_{kl}(\tau)}{d\tau}d\tau$$

$$= \exp\left(-\frac{\Delta t}{\tau_m}\right)h_{ij}^n m + \int_{t_n}^{t_{n+1}} C_{ijkl_m}\exp\left(-\frac{t_{n+1}-\tau}{\tau_m}\right)\frac{d\varepsilon_{kl}(\tau)}{d\tau}d\tau \tag{22}$$

If the change in strain in each time interval is assumed to be constant, then we can write:

$$\frac{d\varepsilon_{kl}}{dt} = \frac{\Delta\varepsilon_{kl}}{\Delta t} = \frac{\varepsilon_{kl}^{n+1}-\varepsilon_{kl}^n}{\Delta t} \tag{23}$$

Substitution of (23) into (22) yields:

$$h_{ij}^{n+1}m = \exp\left(-\frac{\Delta t}{\tau_m}\right)h_{ij}^n m + \int_{t_n}^{t_{n+1}} C_{ijkl_m}\exp\left(-\frac{t_{n+1}-\tau}{\tau_m}\right)\frac{\varepsilon_{kl}^{n+1}-\varepsilon_{kl}^n}{\Delta t}d\tau$$

$$= \exp\left(-\frac{\Delta t}{\tau_m}\right)h_{ij}^n m + C_{ijkl_m}\tau_m\left(1-\exp\left(-\frac{\Delta t}{\tau_m}\right)\right)\frac{\varepsilon_{kl}^{n+1}-\varepsilon_{kl}^n}{\Delta t}$$

$$= \exp\left(-\frac{\Delta t}{\tau_m}\right)h_{ij}^n m(t_n) + C_{ijkl_m}\frac{\tau_m}{\Delta t}\left(1-\exp\left(-\frac{\Delta t}{\tau_m}\right)\right)\left[\varepsilon_{kl}^{n+1}-\varepsilon_{kl}^n\right] \tag{24}$$

If we write $A_m = \frac{\tau_m}{\Delta t}\left(1-\exp\left(-\frac{\Delta t}{\tau_m}\right)\right)$, then (24) can be written as

$$h_{ij}^{n+1}m = \exp\left(-\frac{\Delta t}{\tau_m}\right)h_{ij}^n m + A_m C_{ijkl_m}\left[\varepsilon_{kl}^{n+1}-\varepsilon_{kl}^n\right] \tag{25}$$

Note that equation (25) is a recursive function that depends only on the values $h_{ij}^n m$ and ε_{kl}^n from the previous time step to calculate the stress state at the current time step, thus eliminating the requirement to store the entire history of deformation. The components of the stress relaxation stiffness tensor can be expressed in terms of relaxation modulus $E(t)$, shear relaxation modulus $G(t)$ and bulk relaxation modulus $K(t)$ which are the viscoelastic analogues of elastic Young's modulus, shear modulus and bulk modulus, respectively. These viscoelastic moduli are normally obtained via experimentation. To utilise these experimental data in mathematical modelling, the discrete data are usually approximated using a series of decaying exponentials also called Prony series. In this representation, $E(t)$, $G(t)$, and $K(t)$ are typically approximated respectively as:

$$E(t) = E_\infty + \sum_{m=1}^{n} E_m e^{-\frac{t}{\tau_m^E}}, G(t) = G_\infty + \sum_{m=1}^{n} G_m e^{-\frac{t}{\tau_m^G}}, K(t) = K_\infty + \sum_{m=1}^{n} K_m e^{-\frac{t}{\tau_m^K}} \tag{26}$$

where the subscript ∞ designate the equilibrium or elastic response of the viscoelastic material, so that the stiffness relaxation tensors $\mathbf{C}_\infty$ and $\mathbf{C}_m$ in (20) for plane stress condition are respectively given as:

$$\mathbf{C}_\infty = \frac{E_\infty}{1-\nu^2}\begin{bmatrix} 1 & \nu & 0 \\ \nu & 1 & 0 \\ 0 & 0 & \frac{1-\nu}{2} \end{bmatrix}, \mathbf{C}_m = \frac{E_m}{1-\nu^2}\begin{bmatrix} 1 & \nu & 0 \\ \nu & 1 & 0 \\ 0 & 0 & \frac{1-\nu}{2} \end{bmatrix} \tag{27}$$

5. Dynamic properties

Although material properties such as the relaxation modulus arising from the result of static measurement are sufficient to produce useful characteristics of viscoelastic materials, however, to gain deeper insight into certain rheological characteristics of viscoelastic materials sometimes require expressing the mechanical properties in an alternative form. A very popular alternative is the representation of viscoelastic properties in the frequency domains, often termed as dynamic properties. This can be achieved through dynamic mechanical tests or by converting the result of static measurements. In this communication, the robustness of the proposed methodology will be demonstrated by recovering the effective dynamic properties of viscoelastic composites from the effective static properties. Important dynamic parameters of interest in the characterisation of viscoelastic materials are the storage modulus E' and loss modulus E''. The vector sum of the storage and loss moduli is called the complex modulus, and is typically represented as:

$$E^*(t) = E'(t) + E''(t) \tag{28}$$

where E' represents the elastic component of the material response while E'' represents the viscous component. The tangent of the loss angle or phase lag between stress and strain given by:

$$\alpha = \tan(\phi) = \frac{E''}{E'} \tag{29}$$

is called the tangent modulus or loss tangent/damping factor and provides information on the proportion of energy lost during a deformation cycle, thus providing a quantitative means to measure the degree of viscous response in the total response of a material. The storage and loss moduli are respectively given [52] as:

$$E' = E_0\left(\sum_{m=1}^{n}\overline{E}_m + \sum_{m=1}^{n}\overline{E}_m\frac{\tau_m^2\omega^2}{1+\tau_m^2\omega^2}\right) \tag{30}$$

and

$$E'' = E_0\left(\sum_{m=1}^{n}\overline{E}_m\frac{\tau_m\omega}{1+\tau_m^2\omega^2}\right) \tag{31}$$

where $\overline{E}_m = E_m/E_0$ and $E_0 = E(t=0)$ is the instantaneous relaxation modulus.

6. Computational homogenization

In this contribution, a first-order computational homogenization procedure is proposed for a composite made partly or wholly of viscoelastic constituents. The objective is to determine the overall mechanical properties of the composite material. This objective is born out of the need to understand how the microstructure of the composite material

influences its overall behaviour at the macroscale. This information is useful in predicting and optimizing the performance of composite materials. By understanding the relationship between the microstructure and the macroscopic behaviour of composite material, it is possible to design composite materials with specific properties and performance characteristics for a particular application.

This proposed nonlocal homogenization scheme just like most computational homogenization schemes is composed of three main components. The first is the identification of relevant scales in the problem which are usually denoted as microscale and macroscale. Secondly, a localization procedure that involves finding the stress solution of a mechanical model at the microscale given a macrostrain. Lastly, the development of a homogenization rule that yields macroscopic stress based on the micro fields of the stress tensor.

6.1. Definition of scales and homogenization rule

Given a heterogeneous material M composed of more than one constituent phase (at least one of which is viscoelastic), the objective in this nonlocal first-order computational homogenization scheme is to find an equivalent or substitute material $\overline{M}$ that will have the same overall behaviour as M. The approximation of M with $\overline{M}$ is based on two key assumptions. The first is that if the constituent phases in M exhibit linear behaviour, then the response of the effective (substitute) material $\overline{M}$ will likewise be linear [53,54]. Thus, in this regard, the constitutive function that relates stress and strain fields in M^* takes the linear form:

$$\overline{\sigma}_{ij}(t) = \overline{C}_{ijkl}\overline{\varepsilon}_{kl}(t) \tag{32}$$

where $\overline{C}_{ijkl}$ is the time dependent effective stiffness relaxation tensor, and overbar in (32) and elsewhere in this communication indicates field variables associated with the substitute homogeneous material. The substitute homogeneous material $\overline{M}$ will henceforth be designated as the macroscale. The second assumption is that of statistical homogeneity of the composite system M. This means that M exhibits the same average behaviour over any randomly selected subregion that is sufficiently large in comparison with the size of individual microstructural elements or phase such as the size of inclusions [53]. Any such subregion is called a representative volume element (RVE) and represents the microscale for the purpose of this homogenization scheme. Since the average properties of the composite material are the same within the RVE as they are for the entire material, this allows the use of volume average of field over the RVE instead of volume average of fields over the entire material.

Once the implication of linear effective behaviour and statistical homogeneity is granted, the next task is to find the relationship between the microscopic field of stress and strain with their macroscopic counterparts. This is achieved through the application of nonlocal stress and strain average theorems [38]. Consider a heterogeneous body $\mathfrak{B}$ which occupies a region $\overline{\Omega} = \Omega_s \bigcup \Omega_c$ such that Ω_s represents the region where solution is sought and Ω_c represents the boundary region. The average stress and average strain over Ω_s are denoted as $\langle\boldsymbol{\sigma}\rangle$ and $\langle\boldsymbol{\varepsilon}\rangle$, respectively. The nonlocal average stress theorem states that if $\mathfrak{B}$ attains static equilibrium when a constant stress tensor $\overline{\sigma}$ is applied on the boundary domain Ω_c, then the volume average of the stress field in Ω_s is equal to $\overline{\sigma}$, that is:

$$\langle\sigma\rangle = \overline{\sigma} \tag{33}$$

On the other hand, the nonlocal average strain theorem states that if $\mathfrak{B}$ is subjected to displacement on the boundary domain Ω_c which is produced by a constant strain tensor $\overline{\boldsymbol{\varepsilon}}$ such that $\boldsymbol{u}^0 = \overline{\boldsymbol{\varepsilon}}\boldsymbol{x}$ for all $\boldsymbol{x} \in \Omega_c$, then:

$$\langle\boldsymbol{\varepsilon}\rangle = \overline{\boldsymbol{\varepsilon}} \tag{34}$$

where the quantities $\langle\sigma\rangle$ and $\langle\boldsymbol{\varepsilon}\rangle$ are respectively given by:

$$\langle\sigma\rangle = \frac{1}{V_{\Omega_s}}\int_{\Omega_s}\boldsymbol{\sigma}(\mathbf{x}_\mu)dV_{\Omega_s} \tag{35}$$

and

$$\langle\boldsymbol{\varepsilon}\rangle = \frac{1}{V_{\Omega_s}}\int_{\Omega_s}\boldsymbol{\varepsilon}(\mathbf{x}_\mu)dV_{\Omega_s} \tag{36}$$

6.2. Localization and solution of the microscale RVE problem

To ensure that the macroscale homogeneous material $\overline{M}$ can reproduce the behaviour of the original microscale heterogeneous material M, energy equivalence is prescribed between the two materials. This energetic equivalence requires the two material systems to have the same internal energy despite possessing different microstructure. This is achieved by satisfying the nonlocal macrohomogeneity condition [38]:

$$\langle\sigma_{ij}\varepsilon_{ij}\rangle = \overline{\sigma}_{ij}\overline{\varepsilon}_{ij} \tag{37}$$

It was shown in [38] that the macrohomogeneity condition is satisfied by the following statement of nonlocal Hill's lemma:

$$\langle\sigma_{ij}\varepsilon_{ij}\rangle - \overline{\sigma}_{ij}\overline{\varepsilon}_{ij} = \frac{1}{V_{\Omega_s}}\int_{\Omega_c}\left((\sigma_{ik}-\overline{\sigma}_{ik})\mathscr{S}^s_\omega x_k\left(u_i - x_j\overline{\varepsilon}_{ij}\right)\right)dV_{\Omega_c} \tag{38}$$

where $\mathscr{S}^s_\omega$ denotes a weighted nonlocal gradient operator, $\omega(\boldsymbol{x},\boldsymbol{x}') : \mathbb{R}^n \times \mathbb{R}^n \to \mathbb{R}^+$ is a weight function and the superscript S implies that $\mathscr{S}$ is a symmetric gradient operator (please see [38,55] for detailed explanation on nonlocal gradient operator and general element of nonlocal vector calculus). The Hill's lemma (38) is satisfied by prescribing appropriate boundary conditions [38]. These include application of homogeneous displacement, homogeneous stress, and periodic volume constraint conditions (See [38,56] for discussion on volume constraint arising due to the nonlocal interactions allowed in peridynamics). In this communication, only the homogenous displacement volume constraint condition will receive attention notably because it is the most compatible of the volume constraint conditions with the peridynamic framework and the easiest to implement. An appropriate displacement field is applied to the boundary volume of the RVE so that the gradient of the displacement terms of the integrand of the boundary volume integral (38) is vanished. A typical way to achieve this is to apply linear displacement of the form:

$$\boldsymbol{u}(\boldsymbol{x}) = \overline{\boldsymbol{\varepsilon}}\boldsymbol{x}\forall\boldsymbol{x} \in \Omega_c \tag{39}$$

which has been shown [38] to vanish the right-hand side of (38). Equation (39) provides the volume constraint of the microscale problem in terms of field of macro strain. To complete the definition of the computational homogenization scheme, it is necessary to define the

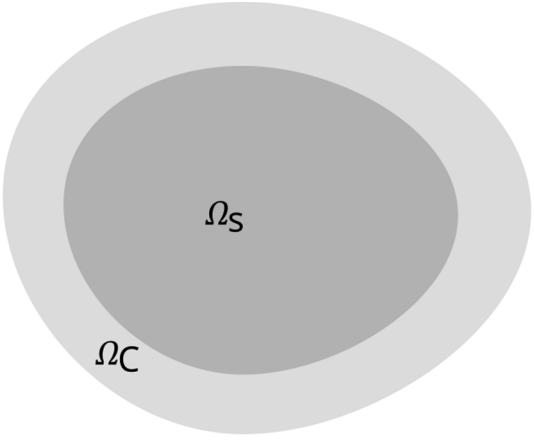

Fig. 2. Micro computational domain showing solution and boundary domains.

microscale volume constraint problem.

6.3. RVE volume constraint problem

Consider the composite material M. Let Ω represents the region occupied by an RVE of M. Let Ω be assumed to be in a state of static equilibrium. To formulate a well-posed microscale VCP, Ω is split into two sub volumes as shown in Fig. 2. The first is Ω_S where solution is sought and the second Ω_C where boundary constraints are imposed. Let $\boldsymbol{\sigma}_\mu$ and $\boldsymbol{\varepsilon}_\mu$ be the micro fields stress and strain in Ω obtained as solution to the following initial volume constraint problem (IVCP):

$$\begin{cases} \int_{\mathscr{B}_\delta(\mathbf{x})} \left[\underline{\mathbf{T}}[\mathbf{x}_\mu]\left\langle \mathbf{x}'_\mu - \mathbf{x}_\mu \right\rangle - \underline{\mathbf{T}}[\mathbf{x}']\left\langle \mathbf{x}_\mu - \mathbf{x}'_\mu \right\rangle\right] d\mathbf{x}'_\mu + \boldsymbol{b}(\mathbf{x}_\mu, t) = 0 & \forall \mathbf{x}_\mu \in \Omega_S \\ \boldsymbol{u}_\mu(\mathbf{x}_\mu) = \boldsymbol{g}_\mu & \forall \mathbf{x}_\mu \in \Omega_C \\ \boldsymbol{u}_\mu(\mathbf{x}_\mu, 0) = \boldsymbol{u}_{\mu(I)} & \forall \mathbf{x}_\mu \in \Omega, \text{for} t = 0 \\ \dot{\boldsymbol{u}}_\mu(\mathbf{x}_\mu, 0) = \dot{\boldsymbol{u}}_{\mu(I)} & \forall \mathbf{x}_\mu \in \Omega, \text{for} t = 0 \end{cases} \tag{40}$$

where the subscript μ in (40) and anywhere else in this communication designate field variables associated with the microscale. The force density vector $\underline{\mathbf{T}}[\bullet_\mu]\langle\bullet\bullet\rangle$ is given by (15) and the response function that relates the micro field stress $\boldsymbol{\sigma}_\mu$ and strain $\boldsymbol{\varepsilon}_\mu$ is given by (18) (for linear material behaviour).

7. Implementation strategy

The proposed homogenization scheme consists of the following steps:

1. This step consists of solving the viscoelastic volume constraint problem (40) at the microscale to obtain the micro fields of stress and strain within the RVE. To do this, a nested spatial and time numerical integration strategy is used. In spatial integration, the total force acting on a material point is evaluated at a given time, while in time integration, material points are tracked over time. Using a meshfree method [62], the spatial integration of the NOSBPD model is numerically implemented using a discrete form of the first of (40) given as

$$\sum_{q=1}^{N}\left[\underline{\mathbf{T}}[\mathbf{x}_p, t]\langle \mathbf{x}_q - \mathbf{x}_p\rangle - \underline{\mathbf{T}}[\mathbf{x}_q, t]\langle \mathbf{x}_p - \mathbf{x}_q\rangle\right] V_q + \boldsymbol{b}_p = 0 \tag{41}$$

where N denotes the total number of material points located within the horizon of the primary material point p. To compute the current accelerations, velocities, and positions of points, the time integration procedure uses the forward Euler method. The explicit time integration of (41) yields the following acceleration, velocity, and displacement at time $t = t^n$:

$$\begin{aligned} \ddot{\boldsymbol{u}}_p^n &= \frac{\mathscr{L}_p^n + \boldsymbol{b}_p}{\rho_p} \\ \dot{\boldsymbol{u}}_p^{n+1} &= \dot{\boldsymbol{u}}_p^n + \ddot{\boldsymbol{u}}_p^n \Delta t \\ \boldsymbol{u}_p^{n+1} &= \boldsymbol{u}_p^n + \dot{\boldsymbol{u}}_p^{n+1} \Delta t \end{aligned} \tag{42}$$

where $\mathscr{L}_p^n = \sum_{q=1}^{N}\left[\underline{\mathbf{T}}[\mathbf{x}_p, t]\langle \mathbf{x}_q - \mathbf{x}_p\rangle - \underline{\mathbf{T}}[\mathbf{x}_q, t]\langle \mathbf{x}_p - \mathbf{x}_q\rangle\right] V_q$. Since the RVE VCP is a quasi-static problem, implementing equation (40) using the forward Euler method will require solving the model as a dynamic problem and then extracting the steady-state solution from the dynamic solution. It is thus proposed in this study to utilize Adaptive Dynamic Relaxation (ADR) [57] to recover the steady state solution of equation (42). This strategy gives rise to two notions of time parameters: a numerical time t_{num} which defines the time necessary for the dynamic solution to converge to the steady-state solution and a material time t_{mat} which is the period over which the viscoelastic response is measured. For numerical implementation, the two times are respectively discretized into interval Δt_{num} and Δt_{mat}.

2. In the second step, macro field stress $\overline{\sigma}_{ij}$ and strain $\overline{\varepsilon}_{ij}$ are obtained as volume averages of the micro fields σ_{ij} and ε_{ij} using (35) and (36). The micro field variables are then utilised in (32) to extract the effective stiffness relaxation tensor $\overline{C}_{ijkl}$.

3. Once the effective stiffness relaxation tensor is obtained, effective viscoelastic material functions such as the effective relaxation modulus $\overline{E}(t)$ and hence $\overline{G}(t)$ and $\overline{K}(t)$ are easily computed. This is usually achieved by assuming constant Poisson's ratio.

4. Prony series (26) is then used to mathematically represent the discrete values of the effective relaxation moduli determined in step 3 above. To achieve this in the present contribution, a least squares curve fitting code was written in MATLAB to determine the coefficients E_∞, E_m and τ_m^E.

5. Dynamic properties such as the storage and loss moduli as well as tangent of phase lag are respectively obtained from (30), (31), and (29).

8. Numerical examples

In this section, the capability of the proposed homogenization scheme to predict the effective properties of composite materials made wholly or partly of viscoelastic materials. To achieve this aim, compu-

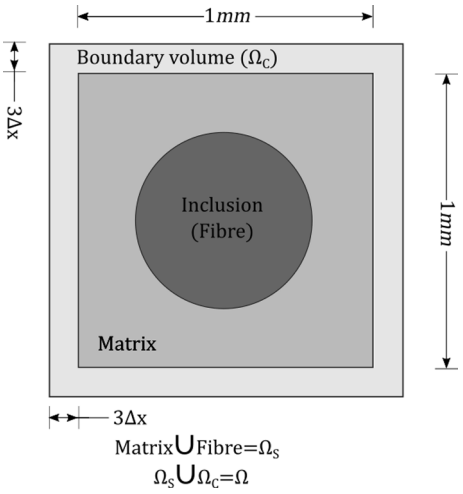

Fig. 3. RVE showing microstructure topology of composites.

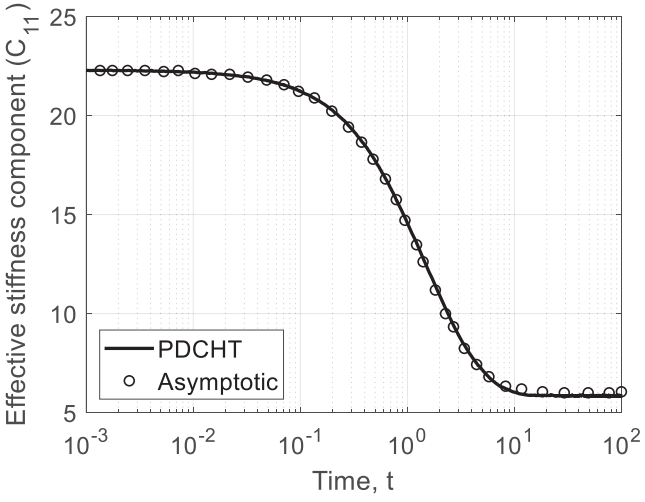

Fig. 4. Effective stress relaxation stiffness tensor. Graph showing the C_{11} component.

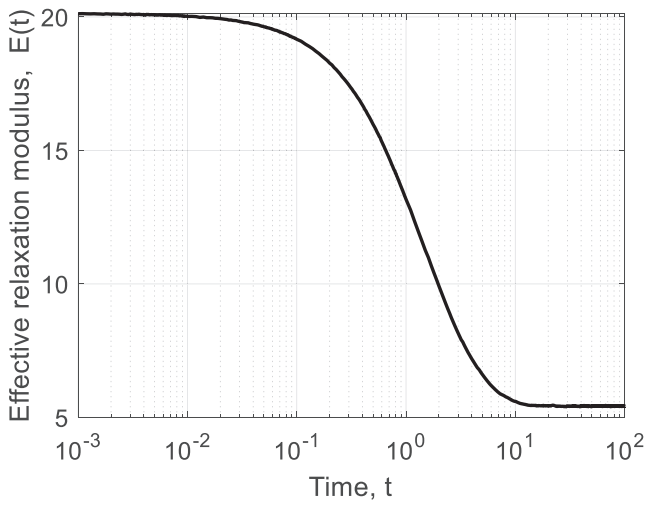

Fig. 5. Effective relaxation modulus obtained from the effective stress relaxation stiffness tensor.

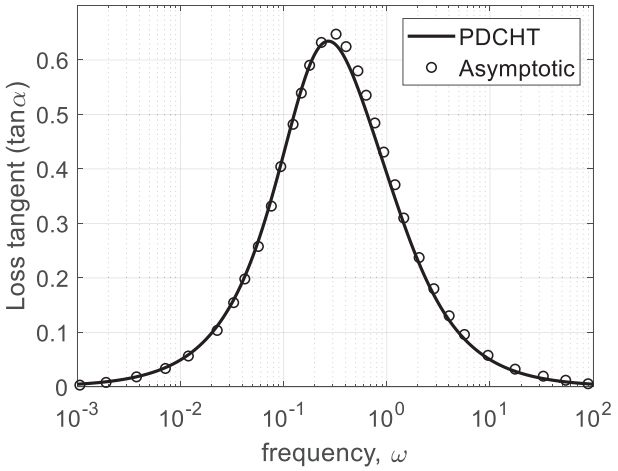

Fig. 6. Effective loss tangent in frequency domain.

tational experiments are carried out to determine the effective material properties of two sets of composite materials. The first is a two-phase matrix-inclusion composite in which one of the phases is elastic and the other viscoelastic. The second is a two-phase matrix-inclusion composite material consisting of a viscoelastic inclusion in a viscoelastic matrix. All numerical experiments are conducted for an inclusion volume fraction of 50%. All computations are carried out under the assumption of plane stress state and that all constituent materials are isotropic and nonaging and the response is measured in the linear regime. The RVE that is representative of the composite materials characterised in this study is shown in Fig. 3.

Table 1
Prony coefficients for effective relaxation modulus data.

Parameter	Fitted value
E_∞	5.4219
E_1	7.5459
E_2	7.1634
τ_1	2.6270
τ_2	0.9876

8.1. Two-phase composite with elastic inclusion and viscoelastic matrix

In this numerical example, the composite consists of an elastic inclusion and viscoelastic matrix as obtained from [5]. The elastic modulus and Poisson's ratio of the inclusion phase are respectively given as $E = 20$ and $\nu = 0.21$, while the relaxation modulus and Poisson's ratio of the inclusion phase are given respectively as $E(t) = 3 + 17\mathrm{e}^{-t}$ and $\nu = 0.38$.

To implement this problem, the RVE is discretised into 100×100 material points. The choice of a horizon size of $3\Delta x$, where Δx represents the length of a material point, was made to facilitate a comparison of the results obtained from peridynamic simulation with those obtained from classical continuum models. It has been previously demonstrated [58] that this horizon size effectively yields results that converge towards the classical solution. Simulation is done with time step $\Delta t_{mat} = 0.01s$ over a total period of $10^3 s$. A numerical time step $\Delta t_{num} = 1s$ is used.

The results of the effective stress relaxation stiffness tensor and effective loss tangent computed using the proposed nonlocal computational homogenization scheme and those computed using an asymptotic homogenization framework [5] are presented in Fig. 4 and Fig. 6, respectively. Fig. 4 shows the effective stress relaxation stiffness tensor computed by both the nonlocal computational homogenization scheme and the asymptotic homogenization scheme over the specified simulation period. It is clear from the figure that the results obtained by the nonlocal computational homogenization scheme closely match those obtained by the asymptotic homogenization framework. This agreement indicates that the proposed nonlocal computational homogenization scheme can accurately predict the time-domain properties of a heterogeneous material, as represented by the component of the effective stress relaxation stiffness tensor.

For further analysis, the effective relaxation modulus of the composite system is extracted from the effective stress relaxation stiffness tensor obtained from the simulation. The effective relaxation modulus obtained is presented in Fig. 5. The data presented in Fig. 5 is curve fitted using the curve fitting code developed in MATLAB to obtain the Prony series coefficients. This allows for the representation of the data in the form (26), which can be useful for further analysis and understanding of the underlying dynamics of the system. The Prony coefficients obtained are presented in Table 1. To compute the effective dynamic properties of the composite system, the coefficients of the effective relaxation modulus obtained above are used in (30) and (31) to compute the storage and loss moduli, respectively. These are then used in (29) to compute the tangent modulus.

Fig. 6 shows the effective loss tangent computed using this proposed

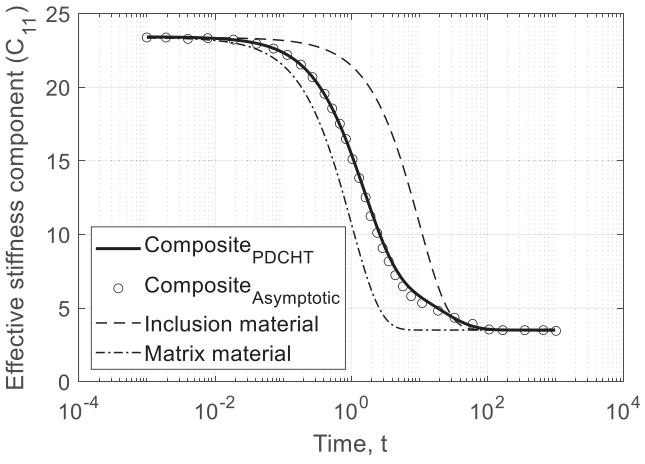

Fig. 7. Component C_{11} of the effective stiffness tensor of a two-phase matrix-inclusion composite system with both matrix and inclusion made of viscoelastic materials.

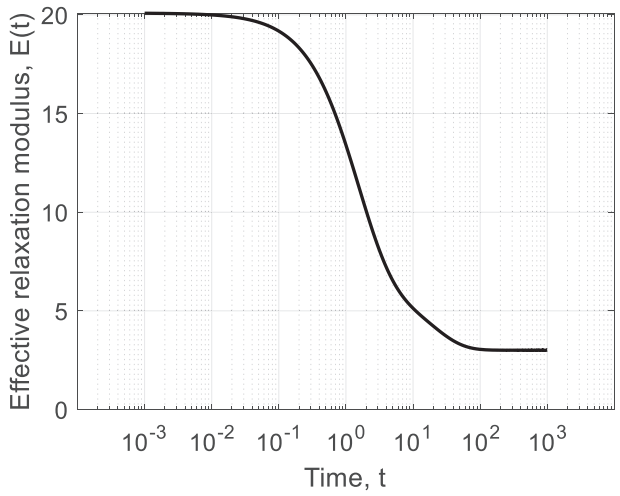

Fig. 8. Effective relaxation modulus of the composite system obtained from the effective stiffness tensor.

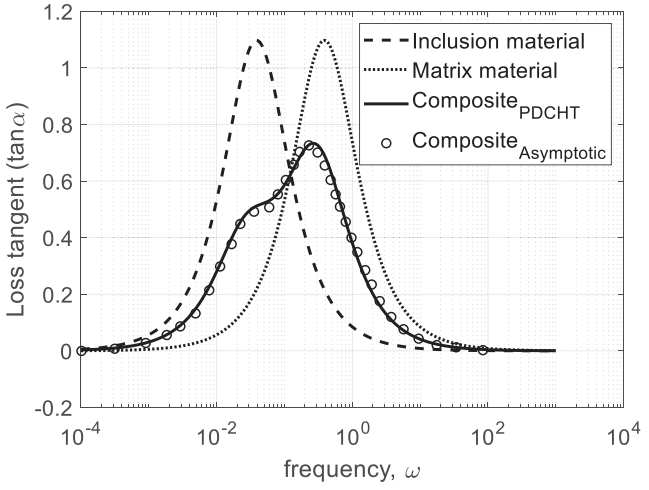

Fig. 9. Effective loss tangent of a two-phase matrix-inclusion composite system made of viscoelastic inclusion and matrix.

Table 2
Coefficients of Prony series representation of effective relaxation modulus.

Parameter	Fitted value
E_∞	3.0
E_1	14.5
E_2	2.5
τ_1	1.7760
τ_2	27.1185

framework and compared with results from [5]. Again, it can be observed that the nonlocal computational homogenization scheme shows good corelation with results obtained by the asymptotic homogenization framework. This agreement demonstrates that the proposed nonlocal computational homogenization scheme can accurately predict the frequency-domain properties of a composite material made of elastic inclusion and viscoelastic matrix, as represented by the effective loss tangent.

8.2. Two-phase composite with viscoelastic inclusion and matrix phases

This example considers a composite with both inclusion and matrix

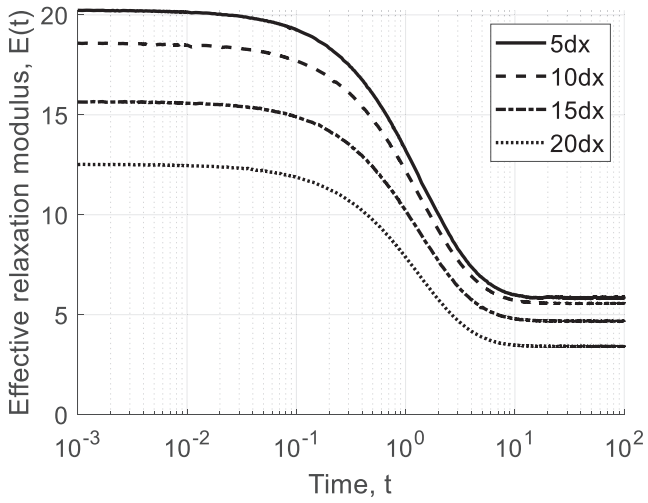

Fig. 10. Effect of nonlocality on the effective relaxation modulus of a two-phase matrix-inclusion composite system.

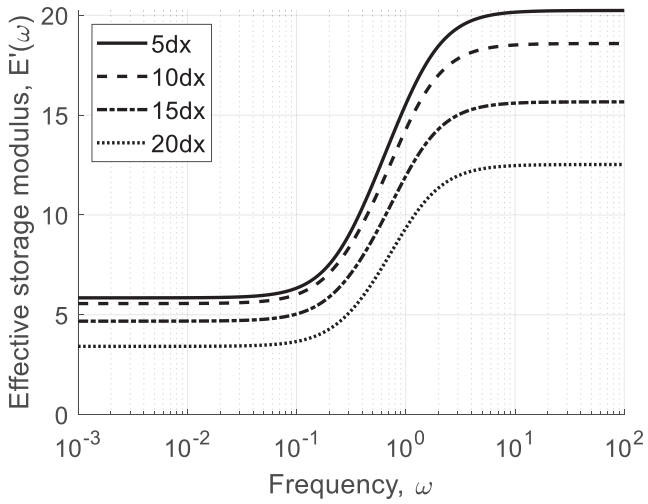

Fig. 11. Effect of nonlocality on the effective loss modulus of a two-phase matrix-inclusion composite system.

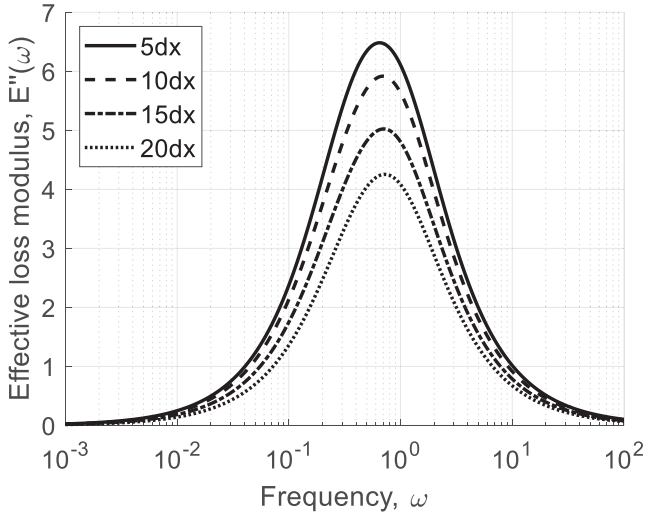

Fig. 12. Effect of nonlocality on the effective storage modulus of a two-phase matrix-inclusion composite system.

phases to be viscoelastic. The material properties are obtained from [5]. The relaxation modulus and Poisson's ratio for the inclusion phase respectively given as $E(t) = 3 + 17e^{-t/10}$ and $\nu = 0.38$ while those for the matrix phase are respectively given as $E(t) = 3 + 17e^{-t}$ and $\nu = 0.38$. The RVE is discretised into 100×100 points, and a horizon size of $3\Delta x$ is used for the same reason stated in 8.1.

The results of the effective stress relaxation stiffness tensor and effective loss tangent for the matrix-inclusion composite made wholly of viscoelastic materials are presented in Fig. 7 and Fig. 9, respectively. These figures compare the results obtained using this proposed nonlocal computational homogenization scheme to those obtained using an asymptotic homogenization framework [5]. Fig. 7 shows a strong correlation between the effective stress relaxation stiffness tensor for the composite material computed using both the nonlocal computational homogenization scheme and the asymptotic homogenization framework over the entire simulation period.

To enable the determination of the effective dynamic properties of this composite system, its effective relaxation modulus is extracted using the procedure stated in 8.1. The effective relaxation modulus is presented as Fig. 8 and the coefficients of the Prony series representation of the effective relaxation modulus as obtained by curve fitting process are presented in Table 2. The Prony series coefficients in Table 2 are utilised to determine the effective loss tangent of the composite system and the result presented in Fig. 9. The effective loss tangent presented in Fig. 9 shows good agreement with result of computation using the asymptotic homogenization in [5]. This demonstrates the capacity of the proposed nonlocal homogenization scheme to accurately predict both time and frequency domain effective characteristics of composites made wholly of viscoelastic constituents.

8.3. *Effect of nonlocality on the effective mechanical properties of composites*

To demonstrate the capacity of the proposed nonlocal homogenization scheme in capturing nonlocal interactions, a parametric study on the composite system presented in 8.1 will be undertaken in this section. The purpose of this study is to investigate the effect of the nonlocal parameter, as represented by the peridynamic horizon δ, on the effective properties of composites in both the time and frequency domains.

The parametric study will involve varying the horizon size, which is the parameter that controls the degree of nonlocal interactions in PD, while keeping all other model parameters fixed. By doing so, it is possible to observe how the effective properties of the composite system change as the degree of nonlocality is varied. To quantify the effect of the horizon size on the effective properties of the viscoelastic composite, the effective stress relaxation modulus, the effective storage modulus, and the effective loss modulus will be calculated for a range of different horizon sizes.

Results of the parametric study on the effect of nonlocal interaction on the effective properties of the viscoelastic composite are presented in Fig. 10, Fig. 11 and Fig. 12. Fig. 10 shows the effective relaxation modulus of the composite for different horizon sizes. The results of the parametric study indicate that as the horizon size, which represents the degree of nonlocal interaction, increases, the effective relaxation modulus decreases. This demonstrates that an increase in nonlocal interaction results in a reduction in the ability of the material to resist stress. This phenomenon can be attributed to the fact that increasing the degree of nonlocality leads to a more diffused stress distribution throughout the material, which results in a lower stress level within the material. As a result, the average value of the stress field is also reduced, leading to a decrease in the effective stiffness of the composite system.

To study the effect of nonlocal interaction on the dynamic properties of the composite, the effective storage and loss moduli were computed over a range of horizon sizes, and the results are presented in Fig. 11 and Fig. 12, respectively. Analysis of these results shows that increasing the nonlocal interaction not only reduces the storage modulus, which is a measure of the resistance of the material to deformation under an applied load, but also the loss modulus, which is a measure of the material's dissipation of energy.

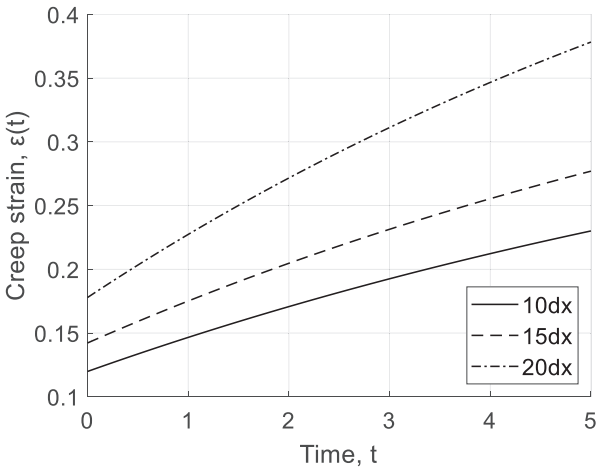

Fig. 13. Creep strain during stress relaxation in a bar for effective relaxation moduli obtained from different degree of nonlocality.

Since nonlocal behaviour is the basis for size effects observed in materials [59], attempts will be made in the following passage to correlate the results of the parametric studies undertaken and presented above with experimental results reported in the literature. When the sample size of a material decreases, the surface to volume ratio increases thus increasing the likelihood of occurrence and relevance of mechanisms occurring at the surface such as crazing in viscoelastic polymer which causes damage and energy dissipation [60] and is also an important mechanism of fracture [61]. In other words, the effect that the specimen size as described by the ratio of surface area to volume has on the behaviour of polymers manifest as size effect which is characterised as nonlocal behaviour. Thus, increasing the surface area to volume ratio can be interpreted as increasing the degree of nonlocal interaction in the material. To be able to compare the implications of results from the parametric studies with experimental observations, a numerical relaxation test to compute the creep strain in a rod of a unit cross-sectional area and unit length is undertaken. The creep strain is computed for material stress relaxation moduli corresponding to horizon sizes $10dx$, $15dx$ and $20dx$ as presented in Fig. 10. Results from these simulations are presented in Fig. 13.

Fig. 13 shows that increasing the horizon size has the effect of increasing the rate of creep as indicated by the increasing steepness of the curve. This behaviour correlate well with result of experiment in [62] in which increasing the ratio of the surface area to volume of polymers was observed to increase the rate of creep for a given applied stress.

9. Conclusion

In this study, a nonlocal computational homogenization scheme, was proposed for determining the effective properties of viscoelastic composite materials using non-ordinary state-based peridynamic theory. The scheme builds on an earlier nonlocal homogenization scheme by introducing a further nonlocality in time through the integral viscoelastic constitutive model. Numerical experiments were carried out on two viscoelastic matrix-inclusion composite systems to demonstrate the capability of the scheme in reproducing results from asymptotic homogenization in the framework of classical continuum mechanics, and good agreement was found between the results from the proposed scheme and those from referenced literature.

In addition to the numerical experiments, a parametric study was

conducted to study the influence of nonlocal interaction on the effective properties of the composite materials. The horizon size was varied while holding other model parameters constant to investigate the effect of varying the degree of nonlocality on the behaviour of the composite system. The results of this parametric study showed that as the degree of nonlocality was increased, the effective behaviour of the composite system became more ductile. This result highlights the importance of accounting for nonlocal interactions when determining the effective properties of viscoelastic composites.

This is especially important with the increasing application of viscoelastic materials in nanocomposites and nanotechnologies. At these small length scales, the significance of nonlocal interactions increases, and thus, it is important to account for these interactions to accurately predict the behaviour of the composite system. This proposed scheme provides a useful tool for understanding the effect of nonlocal interactions on the effective properties of viscoelastic composite materials and could be used as foundation for future studies in this area, especially in the context of nanocomposites and nanotechnologies.

Other potential areas for further research include the application of the proposed scheme to more complex geometries, multiphase systems, and other phenomena that lead to nonlocal interactions such as fracture. Since fracture is inherently a nonlocal process, as such, a nonlocal framework such as the one proposed in this paper is necessary to produce accurate results when analysing viscoelastic composite systems undergoing fracture.

CRediT authorship contribution statement

Yakubu Kasimu Galadima: Conceptualization, Methodology, Software. **Selda Oterkus:** Conceptualization, Methodology, Supervision, Writing – review & editing. **Erkan Oterkus:** Conceptualization, Methodology, Supervision, Writing – review & editing. **Islam Amin:** Conceptualization, Methodology. **Abdel-Hameed El-Aassar:** Conceptualization, Methodology. **Hosam Shawky:** Conceptualization, Methodology.

Declaration of Competing Interest

The authors declare that they have no known competing financial interests or personal relationships that could have appeared to influence the work reported in this paper.

Data availability

Data will be made available on request.

Acknowledgements

The first author is supported by the government of the federal republic of Nigeria through the Petroleum Technology Development Fund (PTDF). This work was supported by a Institutional Links Grant, ID 527426826, under the Egypt-Newton-Mosharafa Fund partnership. The grant is funded by the UK Department for Business, Energy and Industrial Strategy and Science, Technology, and Innovation Funding Authority (STIFA) - Project No. 42717 (An Integrated Smart System of Ultrafiltration, Photocatalysis, Thermal Desalination for Wastewater Treatment) and delivered by the British.

Data availability

The raw/processed data required to reproduce these findings cannot be shared at this time as the data also forms part of an ongoing study.

References

[1] Michel JC, Moulinec H, Suquet P. Effective properties of composite materials with periodic microstructure: a computational approach. Comput Methods Appl Mech Eng 1999;172(1):109–43.
[2] Feyel F, Chaboche J-L. FE2 multiscale approach for modelling the elastoviscoplastic behaviour of long fibre SiC/Ti composite materials. Comput Methods Appl Mech Eng 2000;183(3):309–30.
[3] Petracca M, Pelà L, Rossi R, Oller S, Camata G, Spacone E. Multiscale computational first order homogenization of thick shells for the analysis of out-of-plane loaded masonry walls. Comput Methods Appl Mech Eng 2017;315:273–301.
[4] Tran AB, Yvonnet J, He QC, Toulemonde C, Sanahuja J. A simple computational homogenization method for structures made of linear heterogeneous viscoelastic materials. Comput Methods Appl Mech Eng 2011;200(45):2956–70.
[5] Yi Y-M, Park S-H, Youn S-K. Asymptotic homogenization of viscoelastic composites with periodic microstructures. Int J Solids Struct 1998;35(17):2039–55.
[6] Silling SA. Reformulation of elasticity theory for discontinuities and long-range forces. J Mech Phys Solids 2000;48(1):175–209.
[7] Jirásek M. Nonlocal models for damage and fracture: Comparison of approaches. Int J Solids Struct 1998;35(31):4133–45.
[8] Bažant ZP. Instability, Ductility, and Size Effect in Strain-Softening Concrete. J Eng Mech Div 1976;102(2):331–44.
[9] Fleck NA, Muller GM, Ashby MF, Hutchinson JW. Strain gradient plasticity: Theory and experiment. Acta Metall Mater 1994;42(2):475–87.
[10] Candaş A, Oterkus E, İmrak CE. Dynamic Crack Propagation and Its Interaction With Micro-Cracks in an Impact Problem. J Eng Mater Technol 2020;143(1).
[11] Oterkus E, Madenci E. Peridynamic Theory for Damage Initiation and Growth in Composite Laminate. Key Eng Mater 2012;488–489:355–8.
[12] Askari E, Bobaru F, Lehoucq RB, Parks ML, Silling SA, Weckner O. Peridynamics for multiscale materials modeling. J Phys Conf Ser 2008;125(1):012078.
[13] Madenci E, Oterkus S. Ordinary state-based peridynamics for thermoviscoelastic deformation. Eng Fract Mech 2017;175:31–45.
[14] Hobbs M, Dodwell T, Hattori G, Orr J. An examination of the size effect in quasi-brittle materials using a bond-based peridynamic model. Eng Struct 2022;262:114207.
[15] De Meo D, Oterkus E. Finite element implementation of a peridynamic pitting corrosion damage model. Ocean Eng 2017;135:76–83.
[16] De Meo D, Russo L, Oterkus E. Modeling of the Onset, Propagation, and Interaction of Multiple Cracks Generated From Corrosion Pits by Using Peridynamics. J Eng Mater Technol 2017;139.
[17] Heo J, Yang Z, Xia W, Oterkus S, Oterkus E. Free vibration analysis of cracked plates using peridynamics. Ships Offshore Struct 2020;15(sup1):S220–9.
[18] Javili A, Morasata R, Oterkus E, Oterkus S. Peridynamics review. Math Mech Solids 2019;24(11):3714–39.
[19] Karpenko O, Oterkus S, Oterkus E. Peridynamic investigation of the effect of porosity on fatigue nucleation for additively manufactured titanium alloy Ti6Al4V. Theor Appl Fract Mech 2021;112:102925.
[20] Kefal A, Oterkus E. Displacement and stress monitoring of a chemical tanker based on inverse finite element method. Ocean Eng 2016;112:33–46.
[21] Nguyen CT, Oterkus S, Oterkus E. An energy-based peridynamic model for fatigue cracking. Eng Fract Mech 2021;241:107373.
[22] Oterkus E. Peridynamic Theory for Modeling Three-Dimensional Damage Growth in Metallic and Composite Structures. 2010, The University of Arizona.
[23] Oterkus E, Madenci E, Weckner O, Silling S, Bogert P, Tessler A. Combined finite element and peridynamic analyses for predicting failure in a stiffened composite curved panel with a central slot. Compos Struct 2012;94(3):839–50.
[24] Vazic B, Oterkus E, Oterkus S. Peridynamic Model for a Mindlin Plate Resting on a Winkler Elastic Foundation. J Peridyn Nonlocal Model 2020;2(3):229–42.
[25] Vazic B, Wang H, Diyaroglu C, Oterkus S, Oterkus E. Dynamic propagation of a macrocrack interacting with parallel small cracks. AIMS Mater Sci 2017;4(1):118–36.
[26] Wang H, Oterkus E, Oterkus S. Three-Dimensional Peridynamic Model for Predicting Fracture Evolution during the Lithiation Process. 2018.
[27] Yang Z, Vazic B, Diyaroglu C, Oterkus E, Oterkus S. A Kirchhoff plate formulation in a state-based peridynamic framework. Math Mech Solids 2020;25(3):727–38.
[28] Galadima Y, Oterkus E, Oterkus S. Two-dimensional implementation of the coarsening method for linear peridynamics. AIMS Mater Sci 2019;6(2):252–75.
[29] Galadima YK, Oterkus E, Oterkus S. Model order reduction of linear peridynamic systems using static condensation. Math Mech Solids 2021;26(4):552–69.
[30] Galadima YK, Oterkus E, Oterkus S. Static condensation of peridynamic heat conduction model. Math Mech Solids 2022;27(12):2689–714.
[31] Galadima YK, Xia W, Oterkus E, Oterkus S. Chapter 17 - Multiscale modeling with peridynamics. In: Oterkus E, Oterkus S, Madenci E, editors. Peridynamic Modeling, Numerical Techniques, and Applications. Elsevier; 2021. p. 371–86.
[32] Dorduncu M, Olmus I, Rabczuk T. A peridynamic approach for modeling of two dimensional functionally graded plates. Compos Struct 2022;279:114743.
[33] Dorduncu M, Kutlu A, Madenci E, Rabczuk T. Nonlocal modeling of bi-material and modulus graded plates using peridynamic differential operator. Eng Comput 2023;39(1):893–909.
[34] Dorduncu M, Barut A, Madenci E. Peridynamic Truss Element for Viscoelastic Deformation. In: 57th AIAA/ASCE/AHS/ASC Structures, Structural Dynamics, and Materials Conference.
[35] Madenci E, Barut A, Phan N. Peridynamic unit cell homogenization for thermoelastic properties of heterogenous microstructures with defects. Compos Struct 2018;188:104–15.

[36] Xia W, Galadima YK, Oterkus E, Oterkus S. Representative volume element homogenization of a composite material by using bond-based peridynamics. J Compos Biodegrad Polym 2019;7:51–6.
[37] Xia W, Oterkus E, Oterkus S. Ordinary state-based peridynamic homogenization of periodic micro-structured materials. Theor Appl Fract Mech 2021;113:102960.
[38] Galadima YK, Xia W, Oterkus E, Oterkus S. A computational homogenization framework for non-ordinary state-based peridynamics. Eng Comput 2023;39(1):461–87.
[39] Galadima YK, Xia W, Oterkus E, Oterkus S. Peridynamic computational homogenization theory for materials with evolving microstructure and damage. Eng Comput 2022.
[40] Laurien M, Javili A, Steinmann P. Peridynamic modeling of nonlocal degrading interfaces in composites. Forces Mech 2023;10:100124.
[41] Laurien M, Javili A, Steinmann P. Nonlocal wrinkling instabilities in bilayered systems using peridynamics. Comput Mech 2021;68(5):1023–37.
[42] Silling SA, Epton M, Weckner O, Xu J, Askari E. Peridynamic States and Constitutive Modeling. J Elast 2007;88(2):151–84.
[43] Warren TL, Silling SA, Askari A, Weckner O, Epton MA, Xu J. A non-ordinary state-based peridynamic method to model solid material deformation and fracture. Int J Solids Struct 2009;46(5):1186–95.
[44] Tupek MR, Radovitzky R. An extended constitutive correspondence formulation of peridynamics based on nonlinear bond-strain measures. J Mech Phys Solids 2014;65:82–92.
[45] Wu CT, Ren B. A stabilized non-ordinary state-based peridynamics for the nonlocal ductile material failure analysis in metal machining process. Comput Methods Appl Mech Eng 2015;291:197–215.
[46] Gu X, Madenci E, Zhang Q. Revisit of non-ordinary state-based peridynamics. Eng Fract Mech 2018;190:31–52.
[47] Madenci E, Dorduncu M, Phan N, Gu X. Weak form of bond-associated non-ordinary state-based peridynamics free of zero energy modes with uniform or non-uniform discretization. Eng Fract Mech 2019;218:106613.
[48] Littlewood DJ. Simulation of Dynamic Fracture Using Peridynamics, Finite Element Modeling, and Contact. ASME 2010 International Mechanical Engineering Congress and Exposition. 2010.
[49] Li P, Hao ZM, Zhen WQ. A stabilized non-ordinary state-based peridynamic model. Comput Methods Appl Mech Eng 2018;339:262–80.
[50] Luo J, Sundararaghavan V. Stress-point method for stabilizing zero-energy modes in non-ordinary state-based peridynamics. Int J Solids Struct 2018;150:197–207.
[51] Silling SA. Stability of peridynamic correspondence material models and their particle discretizations. Comput Methods Appl Mech Eng 2017;322:42–57.
[52] Kaliske M, Rothert H. Formulation and implementation of three-dimensional viscoelasticity at small and finite strains. Comput Mech 1997;19(3):228–39.
[53] Hashin Z. Viscoelastic Behavior of Heterogeneous Media. J Appl Mech 1965;32(3):630–6.
[54] Christensen RM. Viscoelastic properties of heterogeneous media. J Mech Phys Solids 1969;17(1):23–41.
[55] Du QIANG, Gunzburger MAX, Lehoucq RB, Zhou KUN. A Nonlocal Vector Calculus, Nonlocal Volume-Constrained Problems, and Nonlocal Balance Laws. Math Models Methods Appl Sci 2013;23(03):493–540.
[56] Buryachenko VA. Computational homogenization in linear elasticity of peristatic periodic structure composites. Math Mech Solids 2019;24(8):2497–525.
[57] Madenci E, Oterkus E, Theory P, Applications I. New York. New York: United States Springer; 2014.
[58] Silling SA, Askari E. A meshfree method based on the peridynamic model of solid mechanics. Comput Struct 2005;83(17):1526–35.
[59] Bažant ZP. Size effect. Int J Solids Struct 2000;37(1):69–80.
[60] Jie M, Tang CY, Li YP, Li CC. Damage evolution and energy dissipation of polymers with crazes. Theor Appl Fract Mech 1998;28(3):165–74.
[61] Van Krevelen DW, Te Nijenhuis K. Chapter 13 - Mechanical Properties of Solid Polymers. In: Van Krevelen DW, Te Nijenhuis K, editors. Properties of Polymers (Fourth Edition). Amsterdam: Elsevier; 2009. p. 383–503.
[62] Wu JBC, Brown N. The effect of specimen size on the mechanical behaviour associated with crazing. J Mater Sci 1977;12(8):1527–34.